International Journal of Biological Macromolecules 164 (2020) 1164–1173

Contents lists available at ScienceDirect

International Journal of Biological Macromolecules

journal homepage: http://www.elsevier.com/locate/ijbiomac

Investigation on *Mecynorhina torquata* Drury, 1782 (Coleoptera, Cetoniidae, Goliathini) cuticle: Surface properties, chitin and chitosan extraction

Tanguy Marmier [a,b], Caroline R. Szczepanski [c], Christophe Candet [d], Arnaud Zenerino [b], René-Paul Godeau [a,b], Guilhem Godeau [a,b,*]

[a] Université Côte d'Azur, INPHYNI, UMR 7010, 06000 Nice, France
[b] Université Côte d'Azur, IMREDD, 06200 Nice, France
[c] Department of Chemical Engineering and Materials Science, Michigan State University, East Lansing, MI 48824, USA
[d] Parc Phoenix, 405 promenade des anglais, 06200 Nice, France

ARTICLE INFO

Article history:
Received 14 March 2020
Received in revised form 19 June 2020
Accepted 13 July 2020
Available online 20 July 2020

Keywords:
Mecynorhina Beetle
Biopolymer extraction
Chitin
Chitosan
Hydrogel formation

ABSTRACT

Naturally derived polymers, such as cellulose or chitin, are materials with increasing interest for a sustainable future. Considering the pollution associated with plastics recycling, natural and fully biocompatible materials like cellulose and chitin are becoming increasingly more relevant for sustainable engineering applications. Chitin and highly deacetylated chitin (chitosan) are already implemented in a wide range of materials applications, especially in biomedical fields. One interesting aspect of chitin is that the majority of industrially produced chitin is extracted from shrimp exoskeleton. However, other arthropods can also be investigated as a source of chitin. In this work, we focus on the extraction of chitin and preparation of chitosan from a beetle specie: *Mecynorhina torquata*. This includes characterization of the native *Mecynorhina torquata* surfaces and all intermediate surfaces throughout the chitosan extraction procedure. The final product, prepared chitosan, is also characterized using IR, SEM, ash content, and deacetylation degree. In addition, spectacular iridescent surfaces of *Mecynorhina torquata* are highlighted at the intermediate steps during chitin extraction. Finally, as proof of concept, the isolated chitosan is used to form hydrogel.

1. Introduction

Chitin is a linear polymer of β-1,4 linked *N*-acetylglucosamine and is the second most abundant biopolymer found in nature. As examples, beetle cuticles, fungi cell walls and crustacean exoskeletons are all naturally rich in chitin. Industrially, the majority of chitin is extracted from seafood products including shrimp, lobster, and crab [1–7]. Chitin has a macromolecular organization rich with strong intramolecular interactions that both increases stability and also lowers chitin solubility in water [8]. Deacetylation of chitin produces chitosan, and the term chitosan is typically reserved for chitin with a deacetylation degree greater than 50% [9]. After deacetylation, chitosan has free amine functional groups that lead to complete solubility in acidic water. Due to this improved solubility, biocompatibility, and biodegradability, chitosan is used for a wide range of applications in food, medicine, and textile as reported in numerous reviews [10–15]. Amongst the numerous uses of chitosan, hydrogel formation is of significant interest. Chitosan hydrogels are used in tissue engineering, the development of injectable materials, wound healing as well as implants [16–21].

Given that the majority of chitin production arises from seafood waste, new sources of chitin are now being investigated such as squid, coral, fungus or insects [20–31]. Simultaneously, insects are being increasingly considered as protein source to feed animals and human, as they have certain advantages. Mainly, insect proteins are of good quality and need minimal space and water for their production. Furthermore, the production of insect proteins produces fewer greenhouse gases compared to production of classical animal proteins [32,33]. These trends make the development of insects a promising avenue for sustainable development. However, similar to seafood, large scale beetle consumption will produce waste, and just as for shrimp, lobster and crab, the waste from beetle protein production will require treatment. One possibility to create value from this industrial waste is to extract chitin and prepare chitosan. In this work, we investigate the possibility of using large bodied beetles as sources for chitin extraction and chitosan development.

Since 2017, our team has studied the potential use of beetles for biosourced materials and bio-inspiration [34–36]. Our work thus far has focused on the wettability and morphology of the beetle shell surface. As

* Corresponding author at: Université Côte d'Azur, INPHYNI, UMR 7010, 06000 Nice, France.
E-mail address: guilhem.godeau@univ-cotedazur.fr (G. Godeau).

https://doi.org/10.1016/j.ijbiomac.2020.07.155
0141-8130/

an example, in 2019 we reported on surface wettability and microstructuration of the *Mecynorhina polyphemus* specie, identifying differences based on gender [37]. In the current report, we focus on a second species from the genus *Mecynorhina*: *M. torquata* (Fig. 1) and investigate the surface morphology and wettability. We also demonstrate how *M. torquata* can be employed for chitin and chitosan development. The *M. torquata* shell is microscopically and macroscopically investigated at each stage of the chitin extraction and chitosan development. The final product, isolated chitosan, is characterized via infrared and thermogravimetric analysis. Ultimately, the isolated chitosan is dissolved in acidic medium and mixed with alginate in order to form a hydrogel.

2. Materials and methods

2.1. Materials

The specimens used in this work were collected from Parc Phoenix (Nice) breeding stock and laboratory stock. The dead specimens were kept in the laboratory stock and the living specimens were kept at Parc Phoenix. Observations were made on 8 specimens (3 males and 5 females). All observations were performed on dried specimens.

2.2. Chitin extraction

Step 1, demineralization: Dry *M. torquata* (5.8 g) was hydrated in a 1 M HCl water solution. The solution was then warmed for 2 h (95 °C). The liquid phase was then removed, and the resulting exoskeleton was rinsed with water until reaching a neutral pH. The exoskeleton was then used in step 2 without any further purification nor drying.

Step 2, deproteination: After finishing Step 1, the exoskeleton was placed in an aqueous 2 M NaOH solution. The solution was then warmed to 95 °C over a period of 36 h. During this treatment, the solution rapidly turned black. Therefore, the NaOH solution was refreshed hourly during the first 6 h of the treatment. The liquid phase was then removed, and the exoskeleton was rinsed with fresh water until achieving a neutral pH and directly used in the next step without further purification nor drying.

Step 3, bleaching: The exoskeleton from Step 2 was bleached using an aqueous H_2O_2 (50 wt%) solution at room temperature for 4 h. The bleached exoskeleton was then washed with water and acetone and finally dried in oven (60 °C), yielding 1.6 g of Chitin (yield 27%).

Fig. 1. Example of *M. torquata* whole specimens.

2.3. Chitin deacetylation (chitosan preparation)

1.57 g of dry chitin was rehydrated in an aqueous NaOH solution (50%, *w*/w). The solution was then warmed (95 °C) overnight. The liquid phase was removed and the solid was washed with fresh water until reaching a neutral pH. The deacetylated chitin (chitosan) was then washed with acetone and dried in an oven at 60 °C. The deacetylation yields 1.42 g (yield: 90%) of chitosan.

2.4. Surface characterization

All surface characterizations were performed on both *M. torquata* native and treated surfaces. All observations were performed in triplicate to obtain standard deviations.

2.4.1. Electronic microscopy

SEM (scanning electron microscopy) observations were carried out using Phenom Pro X Desktop SEM from Thermo Fisher Scientific. Samples were observed with gold coating and at an accelerating voltage of 5 and 10 kV. The samples were coated using Quorum Q150R S Sputter Coater.

2.4.2. NMR characterization

H^1 NMR were performed on a Brucker 400 MHz, using CF_3COOD as solvent. The NMR chemical shifts are reported in ppm. Due to the polymer structure of chitosan, all reported signals are broad signals.

Chitosan from Mecynorhina torquata: δ_H (400 MHz, CF_3COOD, ppm): 2.84 (H—Ac); 4.11 (H2-Deacetylated); 4.25–5.30 (H2 to H6); 5.45–5.65 (H1-Acetylated); 5.70–5.95 (H1-Deacetylated).

2.4.3. FT-IR characterization

Infrared measurements were carried out using a Spectrum Two FT-IR spectrometer from Perkin Elmer with universal ATR accessory. The measurements were performed between 4000 cm^{-1} and 500 cm^{-1}.

2.4.4. Determination of the deacetylation degree of the chitosan [38,39]

Dried chitosan (0.1 g) was dissolved in 30 mL of 0.1 M HCl acid. When chitosan was completely dissolved, solution was titrated with a 0.1 M NaOH solution. Deacetylation degree of chitosan was calculated using the following formula:

$$\text{Deacetylation degree } [\%] = 2.03 * \frac{V2-V1}{m + 0,0042 * (V2-V1.)}$$

where: m is sample mass (g), V1 and V2 are volumes of NaOH solution corresponding to the deflection points respectively for HCl and chitosan hydrochloride, 2.03 is a coefficient resulting from the molecular weight of chitin monomer unit and 0.0042 is a coefficient resulting from the difference between molecular weights of chitin and chitosan monomer units.

2.4.5. TGA and DSC measurements

Thermogravimetric (TGA) and differential scanning calorimetry (DSC) measurements were performed on a TGA STA449 F5 Jupiter ECO from Netzsch. The samples were warmed from 40 °C to 650 °C with heating rate of 20 °C min under nitrogen flow of 50 $mL.min^{-1}$, the temperature was then stabilized at 650 °C over 4 h.

2.4.6. X-ray diffraction (XRD) analysis

X-ray diffraction of powder chitosan samples were examined by Panalytical X'Pert Pro with Xcelerator fast detector operating at 45 kV and 30 mA. The radiation was generated from a Cu Kα (k = 0,15418 nm) source. The diffraction data were collected from 2 h values from 5° to 75°.

The crystallinity index of isolated chitosan samples (CrI) were calculated from XRD data using the following equation [29,40]:

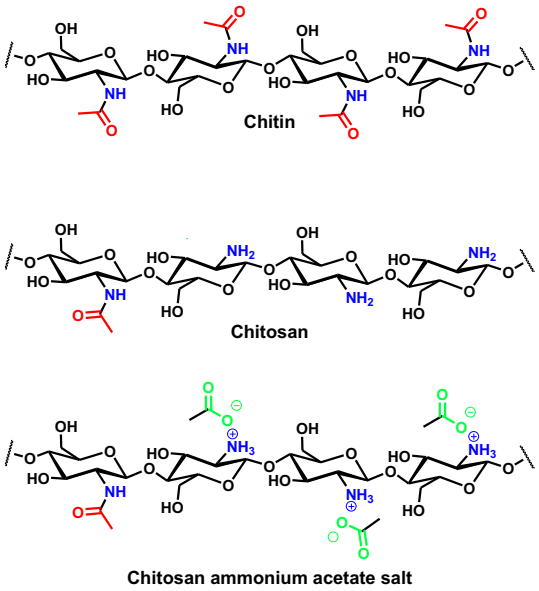

Fig. 2. Theoretical chemical structures of chitin, chitosan and chitosan ammonium acetate salt.

$$CrI = [(I_{cr} - I_{am})/I_{cr}] * 100$$

where I_{cr} is the maximum intensity for crystalline lattices at $2\theta = 19.6°$ and I_{am} is the maximum intensity at $2\theta = 12.6°$ corresponding to the amorphous region.

2.4.7. Elemental analysis

Elemental analysis was carried out on an elemental analyzer Flash EA 1112 series (Thermo Finnigan), driven with Eager Xperience software.

2.4.8. Contact angle measurement

All contact angle measurements were performed on dry insect sections (pronotum and elytra). The apparent and dynamic contact angles were obtained with a DSA10 goniometer (Krüss). The apparent contact angles were measured using the sessile drop method with deionized water drop of 4 μL.

2.4.9. Hydrogel alginate/chitosan preparation

The alginate-chitosan hydrogel was prepared by mixing 5 mL of alginate solution (2% *w*/w, in water) and 5 mL of chitosan solution (2% w/w, in 2% acetic acid solution). One drop of alimentary dye (blue) was added to colour the gel. The mixture was poured into a syringe and then extruded into $CaCl_2$ 0.5 M solution to form viscous, three-dimensional gels. The formed gels were rinsed with distilled water.

3. Results and discussion

3.1. Chitin and chitosan preparation

According to the literature, various strategies can be employed for chitin extraction and chitosan preparation, and most approaches involve chemical or enzymatic treatment [41–44]. Here, we employ a chemical strategy. Chitin is extracted in three steps: 1- demineralisation (1 M HCl aqueous solution, 95 °C, 2 h), 2-deproteination (2 M aqueous NaOH solution, 95 °C, 36 h) and 3- bleaching (50 wt% H_2O_2, RT, 4 h, followed by acetone rinsing). The solid obtained from this procedure is chitin (Fig. 2). After drying, chitin is isolated with 26% yield. This yield is consistent with values obtained for chitin extraction from other beetles in the literature [29].

Chitosan is then obtained after deacetylation of chitin (50/50 *w*/w NaOH water solution, 95 °C, overnight). The final solid is washed with acetone and dried (yield 90%). As illustrated in Fig. 2, the final compound is a poly (β-(1-4)-D-glucosamine) with random presence of *N*-acetyl-D-glucosamine. The isolated chitosan can be fully dissolved in 2% acetic acid solution by forming the chitosan ammonium acetate salt (Fig. 2).

3.2. Macroscopic observations

Important macroscopic variations are observed throughout the different steps of chitin extraction and deacetylation (Fig. 3). Unmodified *M. torquata* presents large green tomentose surfaces with few white spots and lateral white bands (Fig. 1) [45]. Both genders present similar macroscopic surface features and all surface modifications lead to similar macroscopic observations for both genders. Compared with the dry surface (Fig. 3A), the wet *M. torquata* surface presents a metallic aspect (Fig. 3B). This metallic aspect is further exacerbated after surface demineralisation (Fig. 3C). After deproteination, further significant variations are observed (Fig. 3D), as the surface develops a spectacular iridescent aspect. After deproteination, the whole insect body reveals iridescent colours, reflecting turquoise and/or purple depending on the angle of observation (Fig. 4).

This striking change from a tomentose, matte appearance to an iridescent surface is observed after deproteination (Fig. 3D). This effect is well known and characterized for certain insects [46–49], and is a result of the interaction between light and the exposed chitin network. Therefore, it makes sense that surface structural colours are observed upon exposure the chitin network from *M. torquata* cuticle, and the iridescent aspect is preserved as long as the surface is wet. Following deproteination, the hydrogen peroxide treatment only bleaches the

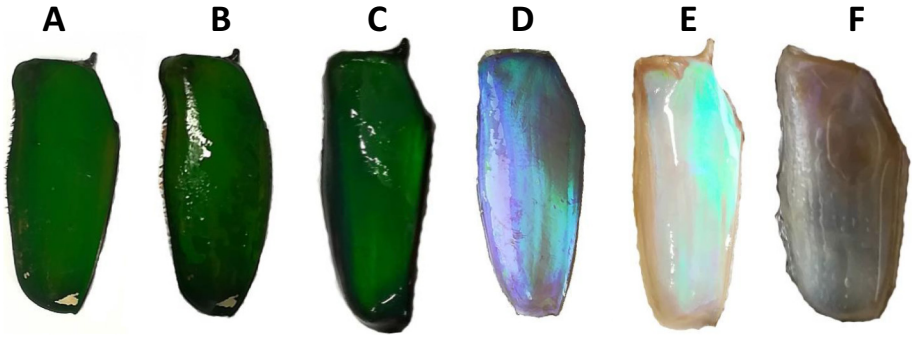

Fig. 3. Macroscopic aspect of *M. torquata* elytra surface. A: native surface, B: wet surface before treatment, C: wet demineralised surface, D: wet deproteinated surface, E: wet bleached surface and F: wet deacetylated surface.

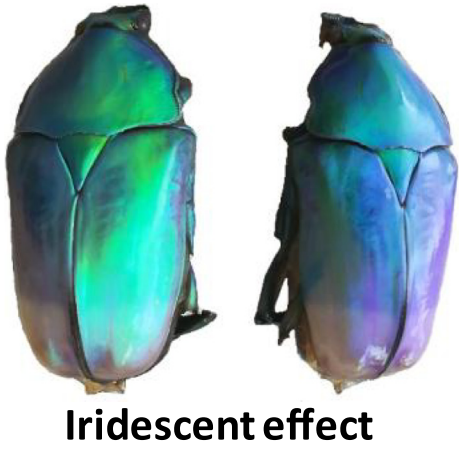

Fig. 4. Colour variation depending on observation angle.

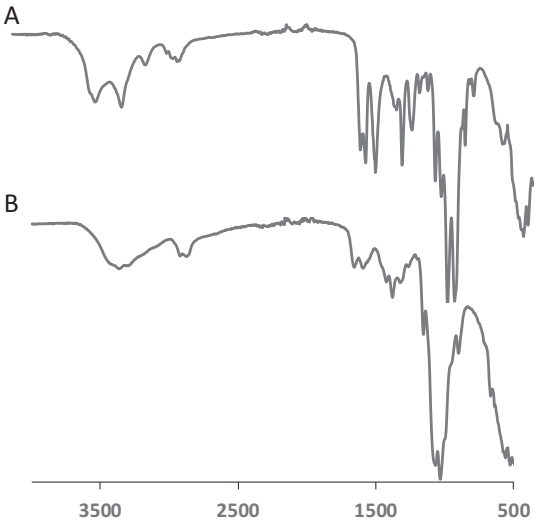

Fig. 5. IR of *M. torquata* chitin (A) and chitosan (B).

surface and thus does not modify the entire chitin network, and therefore the surface maintains a pearly aspect (Fig. 3E). Not surprisingly, the drying of the surface modifies the chitin network. The network may flatten, move or even crack during drying, and therefore the dry surface does not have any iridescence. It is possible to rehydrate the dry specimen, however most of the iridescence is lost since the network cannot spontaneously swell into the proper organization, and therefore the rehydrated surface has a less spectacular optical appearance. After deacetylation, the surfaces are still slightly iridescent, but the optical effect remains weak (Fig. 3F).

3.3. M. torquata chitosan characterisations

To properly characterize the extracted chitin and prepared chitosan, FTIR analysis was conducted. The IR observation shows all the characteristic bands of chitin and chitosan (Fig. 5, Table 1) and the comparison between chitin and chitosan IR reveals some differences.

For chitin (Fig. 5A) strong bands are observed at 3400–3490 cm^{-1} and 3250–3290 cm^{-1}, representing the stretching of O—H and N—H bonds, respectively. Another band is observed at 2850–2900 cm^{-1}, attributed to CH_2 vibration, and two C═O bands corresponding to the amide group are observed at 1615–1665 cm^{-1}. Lastly, the bending and vibration bands from N—H can be observed at 1540–1570 cm^{-1}. Compared with values reported in the literature for chitin extracted from shrimp, all bands observed here are consistent [26]. The C═O band in particular, allows deduction of the M. torquata chitin form. The division of the amide I into two bands near 1650 and 1620 cm^{-1}, indicates that the M. torquata chitin studied here is alpha chitin as described for insect cuticle in literature [42,50].

For chitosan (Fig. 5B) strong bands are observed at 3489–3350 cm^{-1} and 3250–3310 cm^{-1}, corresponding to the stretching of O—H and N—H bonds, respectively. The band corresponding to CH_2 vibration is observed at 2840–2930 cm^{-1} and the C═O band from the amide group is weak but can be observed at 1636–1670 cm^{-1}. Lastly, the bending and vibration bands from N—H can be observed at 1565–1605 cm^{-1}. As expected, the comparison between chitin and chitosan spectra reveals that the IR bands from C═O and N—H amide bonds are significantly weakened in chitosan, demonstrating the efficiency of the deacetylation reaction. As was done with the chitin spectra, the bands observed for chitosan have been compared with data from chitosan derived from shrimp. Again, all reported bands are consistent.

Elemental analysis results of *M. torquata* chitosan are displayed in Table 2. The experimental elemental proportions are all consistent with that expected for chitosan. Both the carbon and hydrogen elemental percentages are quite close to the estimated values for both elements (within 1%), whereas nitrogen is slightly lower (~2%) than the theoretical value.

The deacetylation degree (DD) was estimated using a titration method [38,39]. The titration curve shows two deflections. The first deflection corresponds to excess HCl and the second corresponds to chitosan hydrochloride (Fig. 6). Following this approach, the DD was determined to be 77.6 ± 8.0% for *M. torquata*. This result is consistent with previously published data in the literature for beetles [29].

^{1}H NMR can also be used to confirm the titrated DD (Fig. 7) [51]. Using the following equation, DD is determined by comparing signal integrations of deacetylated and acetylated saccharide units:

$$DD = [H1{-}D/(H1{-}D + 1/3HAc)] * 100$$

In this equation, H1-D is the integration of the proton H1 of deacetylated saccharide (H1-D, integrated to 0.98) and H—Ac is the

Table 2
Elemental analysis for chitosan.

Element	Theoretical values	Experimental values
C	44.6	43.39
H	6.8	6.77
N	8.26	6.64

Table 1
IR data for *M. torquata* and shrimp chitin and chitosan.

Functional group	Commercial chitin [23]	Chitin from *M. torquata*	Commercial chitosan	Chitozan from *M. torquata*
OH stretching	3437 cm^{-1}	3400–3490 cm^{-1}	3340–3380 cm^{-1}	3489–3350 cm^{-1}
NH stretching	3259 cm^{-1}	3250–3290 cm^{-1}	3280–3310 cm^{-1}	3250–3310 cm^{-1}
CH_2 vibration	2867–2937 cm^{-1}	2850–2900 cm^{-1}	2847–2900 cm^{-1}	2840–2930 cm^{-1}
C═O	1620–1654 cm^{-1}	1615–1665 cm^{-1}	1638–1649 cm^{-1}	1636–1670 cm^{-1}
NH (bending)	1553 cm^{-1}	1540–1570 cm^{-1}	1569–1598 cm^{-1}	1565–1605 cm^{-1}

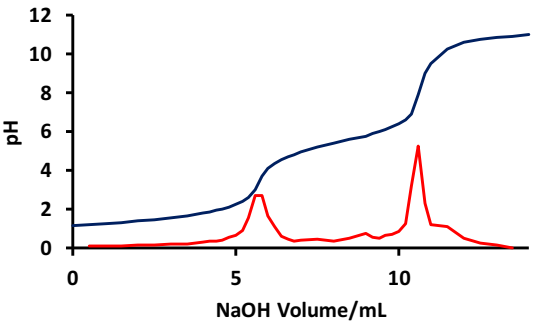

Fig. 6. Example of titration curve for *M. torquata* chitosan deacetylation degree determination.

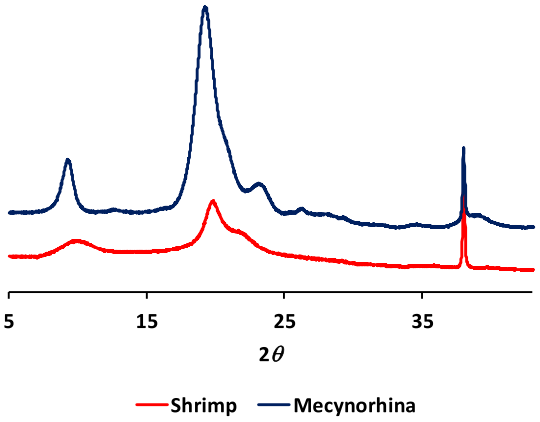

Fig. 8. XRD observation for chitosan (Red: Shrimp and Blue: M. Torquata).

integration of the peak corresponding to the three protons associated with the acetyl group (H—Ac, integrated to 1.0). The DD calculated using NMR is 76,1%. This value is consistent with the DD determined via titration (Fig. 6).

As an additional characterization, X-ray diffraction (XRD) was also employed (Fig. 8) on M. torquata chitosan. The chitosan of M. torquata at 2θ displayed major peaks at 9.3°and 19.2°, with latter having a shoulder at 20.9°, as well as a weak peak at 23.3°. As a comparison, commercially available shrimp chitosan was also investigated. For the shrimp chitosan similar behavior was found as peaks were observed at 9.9° and 19.8°, with a shoulder on the latter at 22.2°. XRD measurements were also used to determine the crystallinity index (CrI). The CrI indices were found to be 83,5% and 53,7% for M. torquata and shrimp, respectively.

3.4. Thermal analysis

In addition to spectroscopic characterization, the thermal behavior of M. torquata chitosan was analysed (Fig. 9). In this experiment, chitosan was slowly heated from 40 to 650 °C and the temperature was maintained at 650 °C over a period of 4 h. The obtained thermal degradation profile is comprised of two steps. The first represents a loss of moisture and is observed up to 100 °C (2% loss) and the second represents decomposition of the chitosan (Fig. 9A).

The DSC curve reveals a chitosan degradation peak at 304 °C (Fig. 9B), and this observation is consistent with the degradation temperature reported for chitosan in the literature [24,25]. After a heating

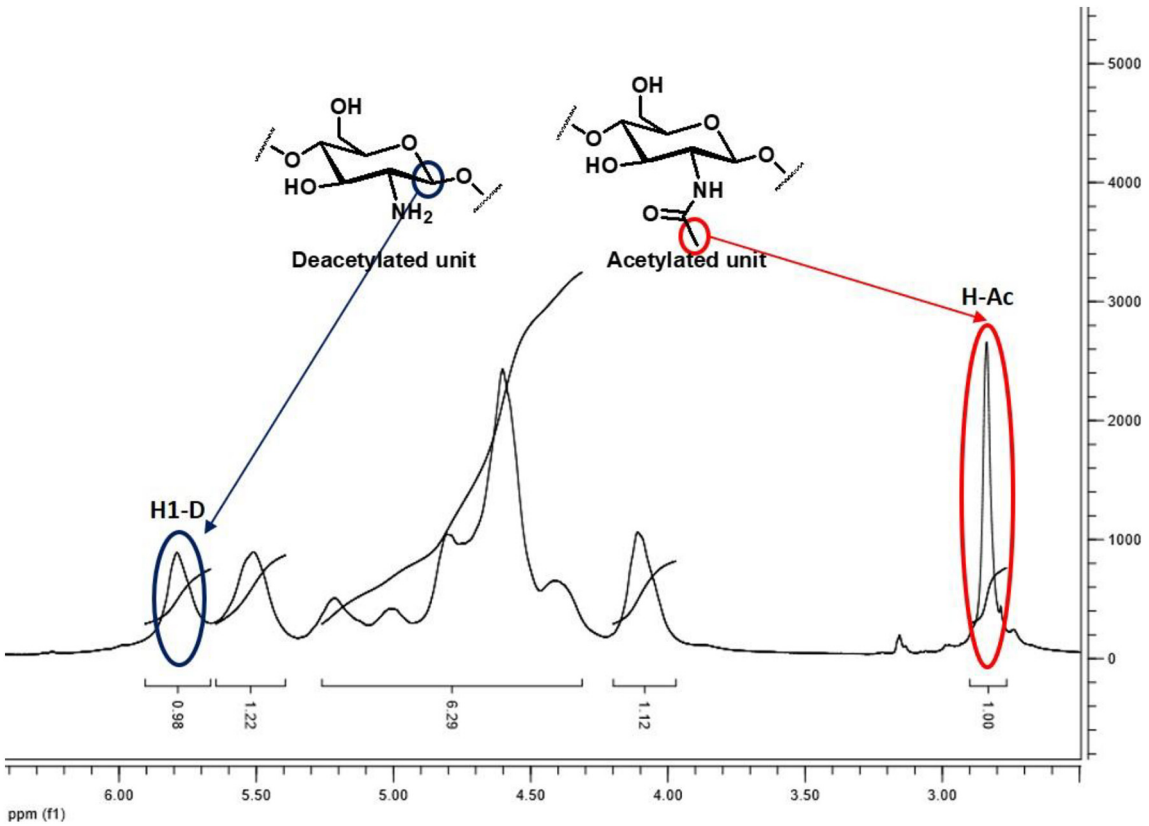

Fig. 7. Example of ^{1}H NMR for M. torquata Chitosan.

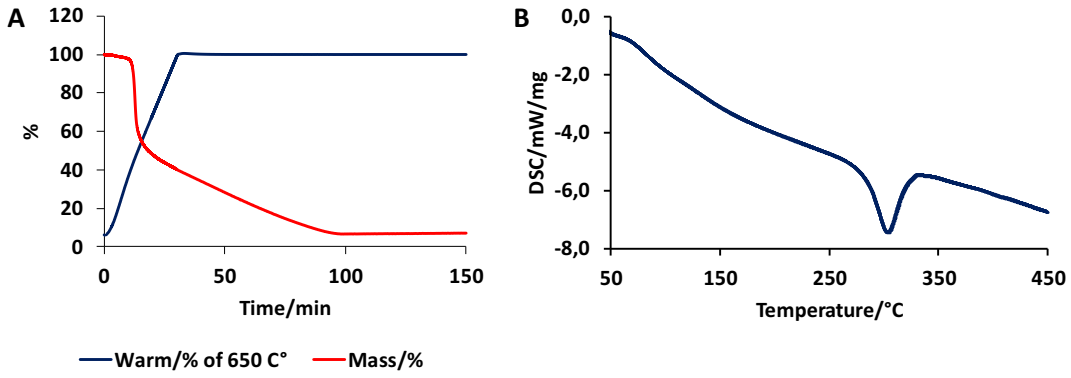

Fig. 9. Thermal analysis for *M. torquata* chitosan. A) TGA observation, B) DSC observation.

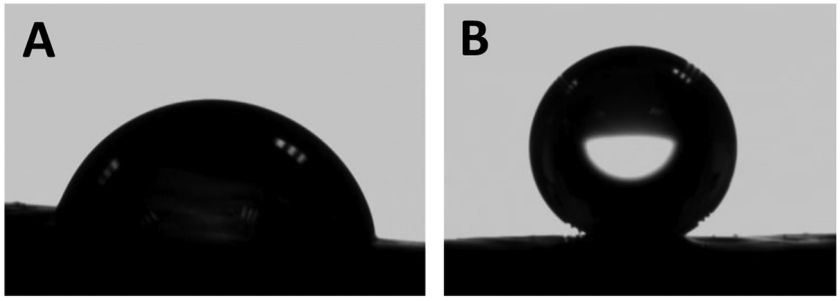

Fig. 10. Example of water drop deposed on *M. torquata* surface. A: female and B: male.

period of 4 h at 650 °C, any remaining mineral matter is comprised of residual ashes. Ash percentage is an important parameter when characterizing chitosan, since ash content may impact chitosan solubility and the viscoelastic properties of the derived material. For many applications of chitosan, particularly the formation of hydrogels, a low ash level is preferred. For M. torquata chitosan, residual ashes were determined to be 7% of the starting mass of sample (Fig. 9A).

The wettability of *M. torquata* surfaces was also investigated, and as in our prior observations of *M. polyphemus* [37], a significant difference in wettability is observed between male and female specimens (Fig. 10). The male surface is highly hydrophobic with an apparent contact angle of $\Theta = 136 \pm 6°$ (Fig. 10B), whereas the female specimen has an apparent contact angle of $\Theta = 66 \pm 11°$, indicating mild hydrophilicity (Fig. 10A). Surface wettability is correlated with two main parameters: surface free energy and surface roughness [53–55]. As specimen of the same species, the surface energies should be similar for each specimen and therefore the observed differences are likely due to variations in roughness. On the male specimen, it is observed that a water droplet deposited onto the surface remains stuck even when tilted to an angle of 90°. This behavior is described as the petal effect, or parahydrophobicity, in the research literature [56–58] and is consistent with wettability previously observed on *M. polyphemus* [37].

Out of curiosity, the wettabilities of all dried, modified surfaces were investigated during the various stages of chitin extraction and chitosan preparation. From these measurements, two observations can be made. First, during the different stages of chitin extraction, differences in wettability between male and female specimens are eliminated. Secondly, hydrophobicity decreases during the process of chitin extraction and chitosan preparation. After demineralization, a significant decrease in hydrophobicity is observed (Fig. 11B), with an apparent contact angle of $\Theta = 91 \pm 3°$ for male and $\Theta = 88 \pm 13°$ female specimens, indicating no significant difference due to gender. After deproteination, the surfaces become dramatically more hydrophilic with an apparent contact angle lower than 30° (Fig. 11C). This increase in the wettability is consistent with the evolution of the surface composition, as it will become more and more polar during the chitin extraction and chitosan preparation.

3.5. Microscopic observations of M. torquata surface

The surface morphology of the various specimens was investigated using scanning electron microscopy (SEM). The initial surfaces of *M. torquata* have generally similar morphologies, regardless of gender. Depending on the green or white section of the surface, two different

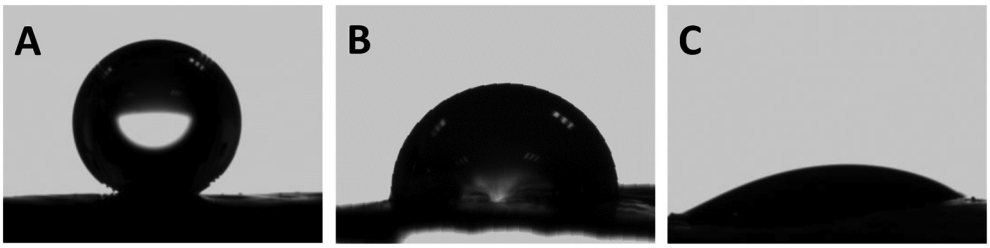

Fig. 11. Example of water drop deposed on *M. torquata* male. A: Native surface, B: demineralised surface and C: deproteinated surface.

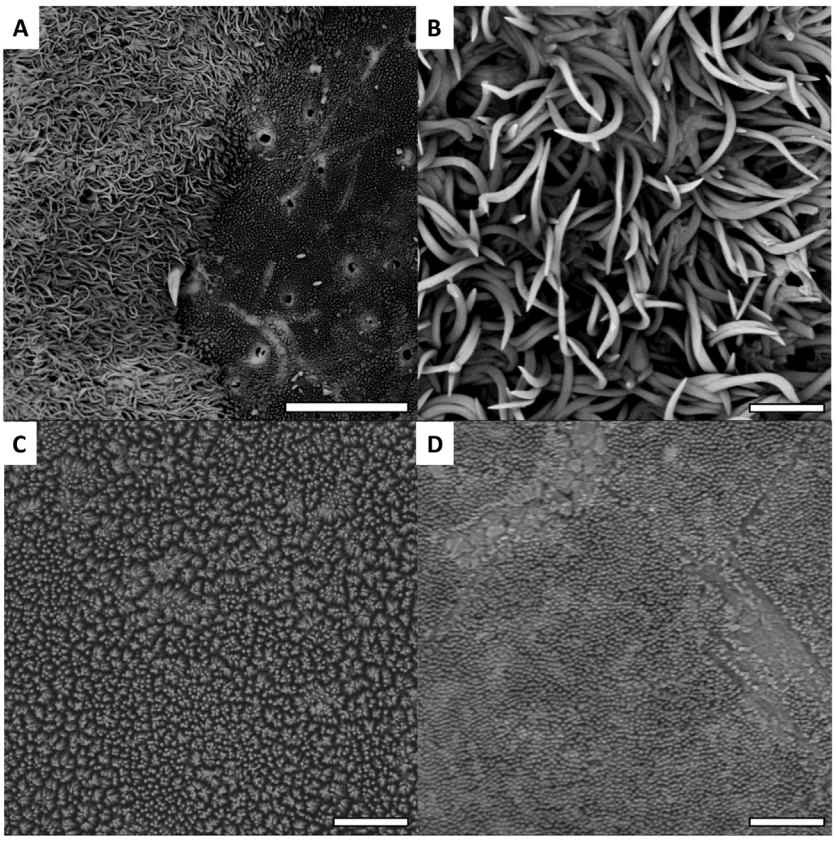

Fig. 12. SEM image of *M. torquata*. A: intersection between green and with part (Scale bar: 80 μm). B: White part (Scale bar: 10 μm). C: Male Green part (Scale bar: 10 μm). D: Female damaged green part (Scale bar: 10 μm).

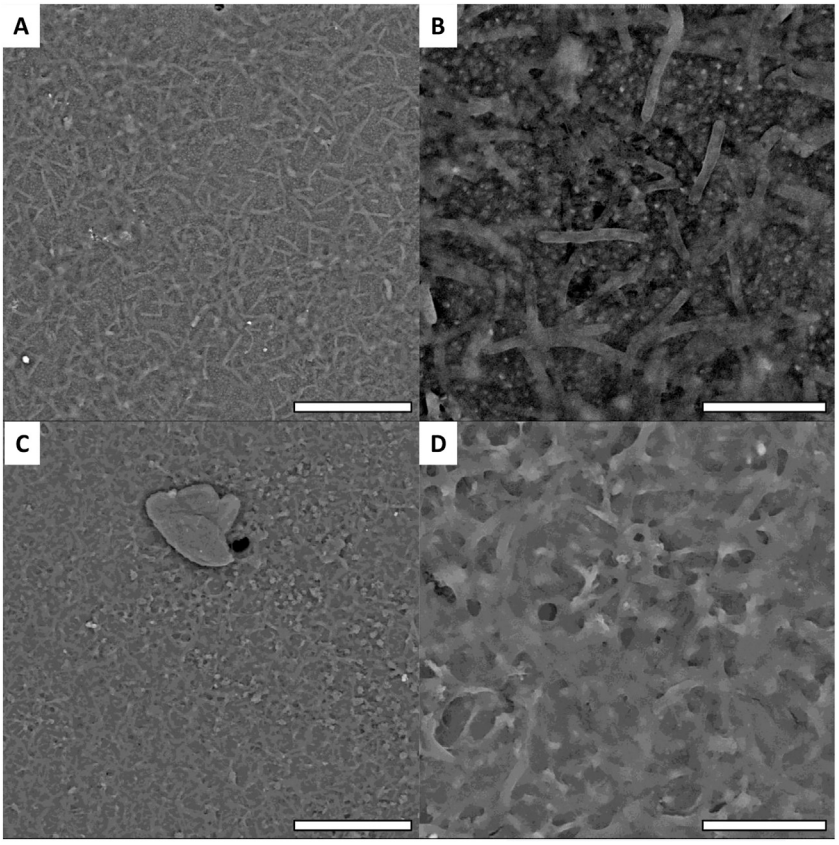

Fig. 13. Example of SEM image for demineralised surface. A and B show image of *M. torqua* white part. C and D show image of *M. torqua* green part. (A and C scale bar: 30 μm and B and D scale bar: 8 μm).

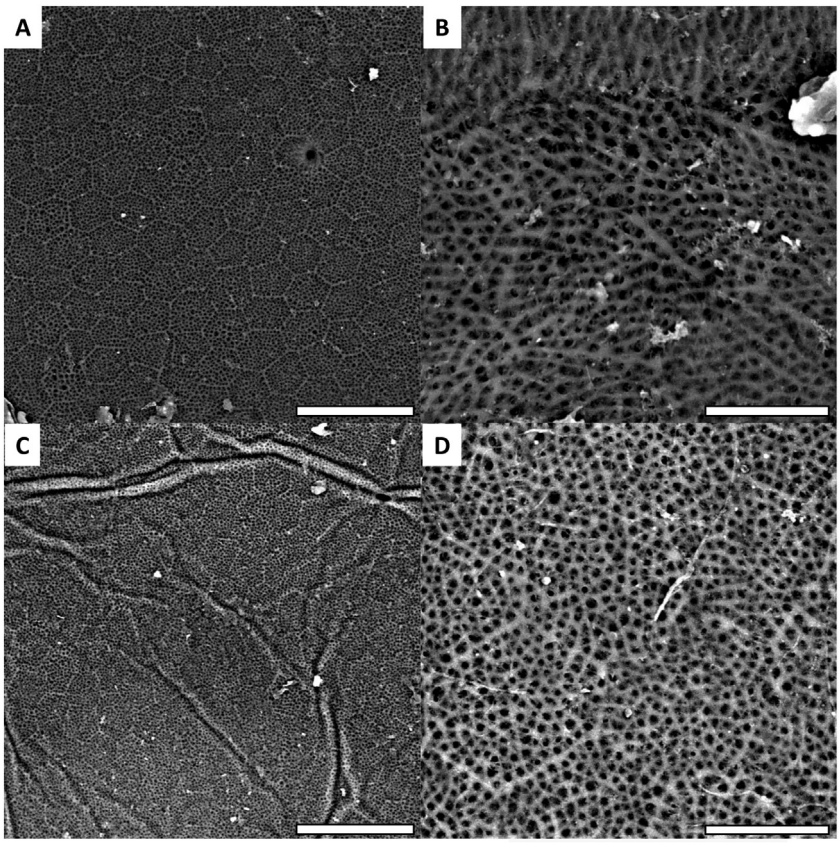

Fig. 14. Example of SEM image for chitin (A: Scale bar: 30 μm and B: Scale bar: 8 μm) and chitosan (C: Scale bar: 30 μm and D: Scale bar: 8 μm).

morphologies were observed (Fig. 12A). The white sections present long, mixed, fiber-like structures (Fig. 12B) and the green sections present short, erect spikes (Fig. 12C). While generally both genders present similar morphologies, subtle differences are observed between the male and female specimens in the green sections. Both present erect spikes, which are well preserved in the case of male specimen, however on the female specimens some damaged areas are observed amongst these erect spikes (Fig. 12D). This difference in surface features between genders can explain the more hydrophilic character observed on the female surface (Fig. 10A). One potential explanation for these differences is that the surface may be damaged by abrasion when the female burrows underground in order to lay eggs.

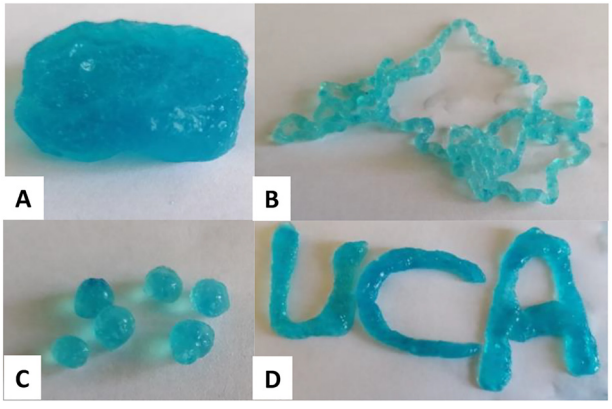

Fig. 15. Example of three-dimensional structures formed with alginate chitosan hydrogel: A. Right block, B. Fibbers, C. Beads and D. Letters.

After demineralisation, the surface morphology evolves significantly. Both white and green sections present less defined morphologies, however it is still possible to distinguish fibers in the white sections (Fig. 13A–B). In the green sections of the specimens (Fig. 13C–D), the damaged and preserved surfaces of the female and male specimens appear much more similar. This observation can explain the similar wettabilities measured for both male and female specimens after demineralisation.

After deproteination, the surfaces reveal a well-defined, ordered network. This morphology does not evolve nor change significantly after bleaching and deacetylation, which is obvious from Fig. 14A–B and C–D, which are SEM images of chitin and chitosan networks, respectively. These networks are consistent with the spectacular iridescent appearance observed for surfaces after deproteination (Fig. 4D) and bleaching (Fig. 4E) as this order contributes to the observed optical effects. However, since we only can image the superficial layer of the chitin network via SEM, it is not possible to conclusively link structural colour to network properties without knowing the organization of all layers of the chitin network.

3.6. Alginate/chitosan hydrogel formation

The extracted *M. torquata*'s chitosan has also been employed to form a hydrogel. Various protocols are reported in the literature for hydrogel development. Amongst these protocols, many report the use of a mixture of chitosan with a secondary polymer, such as polyvinyl alcohol (PVA), polyacrylic acid or sodium alginate [59–61]. The three-dimensional structure of the hydrogel in these examples is typically stabilized using a cross-linking agent. The cross-linking can be covalent in nature (for example, with dicyclohexylcarbodiimide (DCC)) or electrostatically driven, as with calcium chloride ($CaCl_2$) [62,63]. Here, we chose to develop alginate/chitosan hydrogels with calcium chloride as

the cross-linking agent. The hydrogel was formed by mixing sodium alginate solution and *M. torquata* chitosan ammonium acetate solution to form a final alginate (1%)/chitosan (1%) (*w*/w) solution. The prepared mixture was then extruded using a syringe into a calcium chloride solution (0,5 M) in order to stabilize three-dimensional structures (Fig. 15). Utilizing extrusion enables preparation of various 3D morphologies including a rigid block (Fig. 15A), fibers (Fig. 15B), beads (Fig. 15C) and to even write out specific letters (Fig. 15D). As expected, *M. Torquata* chitosan allows stabilization of 3D structures. Of course, these results are preliminary and additional characterization is necessary to determine the perfect conditions for use of beetle chitosan in materials or biomedical applications.

4. Conclusion

In conclusion, we report new observations of *M. torquata* surfaces. We describe the surface morphology and wettability of native surfaces. Furthermore, we explore the use of *M. torquata* specimens for chitin extraction and chitosan preparation. These polysaccharides were obtained using simple, straight-forward chemical treatments including demineralisation, deproteination, bleaching and deacetylation. These treatments revealed spectacular intermediate surfaces with structural iridescence. All surfaces were investigated for their morphologies using SEM. After the four-step process, the treated cuticle produced chitin (26% yield), and after deacetylation chitosan was produced (90% yield). The formed chitosan was characterized via FTIR, TGA, DSC and XRD. The XRD experiments reveal the high crystallinity level of M. torquata chitosan (83.5%). The deacetylation degree was determined to be higher than 75% according to titration and ^{1}H NMR analyses. Thermal analysis reveals a degradation temperature near 304 °C and ash content was measured at 7% using thermogravimetric measurements. All collected data confirms the quality of the extracted chitosan from M. torquata. To confirm the potential utility of the described material, the isolated chitosan was used with alginate to successfully form three-dimensional hydrogels. Of course, this result is just a proof of concept and needs to be elaborated in a future work, but it shows the potential of *M. torquata* chitosan for future biomedical applications. As with shrimp-derived chitosan, insect chitosan has been described as non-toxic and ecofriendly. This type of biosurced material is surely of interest for many industries, including 3D bio-printing as well as biomedical applications.

Author statements

Tanguy Marmier: Investigation
Caroline R. Szczepanski: Writing - Original Draft, Formal analysis
Christophe Candet: Investigation
Arnaud Zenerino: Investigation
René-Paul Godeau: Writing - Original Draft, Conceptualization, Formal analysis
Guilhem Godeau: Investigation, Conceptualization, Funding acquisition, Writing - Original Draft, Project administration, Resources, Formal analysis.

Acknowledgments

This work was supported by the French National Research Agency (ANR, Agence Nationale de la Recherche) as future investment project UCA^{JEDI} with reference: n° ANR-15-IDEX-01. TGA, SEM and contact angle measurements were performed at the Smart City Innovation Center (Université Côte d'Azur, IMREDD). The "Smart City Innovation Center" is a project funded by the European union with the European fund for regional development and co-funded by metropole Nice Côte d'Azur, the département Alpes-maritimes, the région Sud Provence-Alpes-Côte and France for the "initiative d'excellence" (Investissements d'avenir). The authors also thank enterprise Enki eco solutions (Cannes, France) for funding. The group thanks Pr. J. Thibonnet (E.A. 7502, Université de Tours, France) and V. Heresanu Ph. D. (CINaM, UMR 7325 CNRS, Université Aix-Marseille, France), who help for complementary analysis during the COVID-19 pandemic.

References

[1] I. Hamed, F. Ozogul, J.M. Regenstein, Industrial applications of crustacean by-products (chitin, chitosan, and chitooligosaccharides): a review, Trends Food Sci. Technol. 48 (2016) 40–50.
[2] A. Martin, Fisheries waste biomass: bioconversion alternatives, Bioconversion of Waste Materials to Industrial Products, Springer 1998, pp. 449–479.
[3] B.K. Simpson, N. Gagne, M.V. Simpson, Bioprocessing of chitin and chitosan, Fisheries Processing, Springer 1994, pp. 155–173.
[4] R.A. Muzzarelli, Native, industrial and fossil chitins, Chitin and Chitinases, Springer 1999, pp. 1–6.
[5] M. Eddya, B. Tbib, K. EL-Ha, A comparison of chitosan properties after extraction from shrimp shells by diluted and concentrated acids, Heliyon 6 (2020), e03486. .
[6] Y. Lee, H.-W. Kim, Y.H. Brad Kim, New route of chitosan extraction from blue crabs and shrimp shells as flocculants on soybean solutes, Food Sci. Biotechnol. 27 (2018) 461–466.
[7] S. Kheirandish, M. Ghaedi, K. Dashtian, F. Hidari, F. Pourebrahim, S. Wang, Chitosan extraction from lobster shells and its grafted with functionalized MWCNT for simultaneous removal of Pb2+ ions and eriochrome cyanine R dye after their complexation, Int. J. Biol. Macromol. 102 (2017) 181–191.
[8] P. Sikorski, R. Hori, M. Wada, Revisit of α-chitin crystal structure using high resolution X-ray diffraction data, Biomacromolecules 10 (2009) 1100–1105.
[9] A. Tolaimate, J. Desbrieres, M. Rhazi, A. Algui, Contribution to the preparation of chitins and chitosans with controlled physico-chemical properties, Polymer 44 (2003) 7939–7952.
[10] P. Sahariah, M. Másson, Antimicrobial chitosan and chitosan derivatives: a review of the structure−activity relationship, Biomacromolecules 18 (2017) 3846–3868.
[11] H. Yi, L.-Q. Wu, W.E. Bentley, R. Ghodssi, G.W. Rubloff, J.N. Culver, G.F. Payne, Biofabrication with chitosan, Biomacromolecules 6 (2005) 2882–2894.
[12] S. Van Vlierberghe, P. Dubruel, E. Schacht, Biopolymer-based hydrogels as scaffolds for tissue engineering applications: a review, Biomacromolecules 12 (2011) 1387–1408.
[13] H. Wang, J. Qian, F. Ding, Emerging chitosan-based films for food packaging applications, J. Agric. Food Chem. 66 (2018) 395–413.
[14] Shahid-ul-Islam, M. Shahid, F. Mohammad, Green chemistry approaches to develop antimicrobial textiles based on sustainable biopolymers: a review. Ind. Eng. Chem. Res. 52 (2013) 5245–5260.
[15] V.K. Thakur, M.K. Thakur, Recent advances in graft copolymerization and applications of chitosan: a review, ACS Sustain. Chem. Eng. 2 (2014) 2637–2652.
[16] R.V. Badhe, D. Biju kumar, D.R. Chejara, M. Mabrouk, Y.E. Choonara, P. Kumar, L.C. Du Toit, P.P.D. Kondiah, V. Pillay, A composite chitosan-gelatin bi-layered, biomimetic macroporous scaffold for blood vessel tissue engineering, Carbohydr. Polym. 157 (2017) 1215–1225.
[17] K. Xiaoying, F. Jun, S. Kai, W. Lili, L. Xuefang, S. Jinsheng, Biomimetic hydrogel for rapid and scar-free healing of skin wounds inspired by the healing process of oral mucosa, Acta Biomater. 100 (2019) 255–269.
[18] L. Zou, Y. Zhang, X. Liu, J. Chen, Q. Zhang, Biomimetic mineralization on natural and synthetic polymers to prepare hybrid scaffolds for bone tissue engineering, Colloids Surf. B: Biointerfaces 178 (2019) 222–229.
[19] A. Ghaeea, S. Bagheri-Khoulenjanib, H. Amir Afshara, H. Bogheiria, Biomimetic nanocomposite scaffolds based on surface modified PCL-nanofibers containing curcumin embedded in chitosan/gelatin for skin regeneration, Compos. B. Eng. 177 (2019), 107339. .
[20] G. Cao, C. Wang, Y. Fan, X. Li, Biomimetic SIS-based biocomposites with improved biodegradability, antibacterial activity and angiogenesis for abdominal wall repair, Mater. Sci. Eng. C 109 (2020), 110538. .
[21] L.-P. Yan, Y.-J. Wang, L. Ren, G. Wu, S.G. Caridade, J.-B. Fan, L.-Y. Wang, P.-H. Ji, J.-M. Oliveira, J.T. Oliveira, J.F. Mano, R.L. Reis, Genipin-cross-linked collagen/chitosan biomimetic scaffolds for articular cartilage tissue engineering applications, J. Biomed. Mater. Res. A 95A (2010) 465–475.
[22] S. Ifuku, R. Nomura, M. Morimoto, H. Saimoto, Preparation of chitin nanofibers from mushrooms, Materials 4 (2011) 1417–1425.
[23] J. Vetter, Chitin content of cultivated mushrooms *Agaricus bisporus*, *Pleurotus ostreatus* and *Lentinula edodes*, Food Chem. 102 (2007) 6–9.
[24] M. Bo, G. Bavestrello, D. Kurek, S. Paasch, E. Brunner, R. Born, R. Galli, A.L. Stelling, V.N. Sivkov, O.V. Petrova, D. Vyalikh, K. Kummer, S.L. Molodtsov, D. Nowak, J. Nowak, H. Ehrlichc, Isolation and identification of chitin in the black coral Parantipathes larix (Anthozoa: Cnidaria), Int. J. Biol. Macromol. 51 (2012) 129–137.
[25] M. Kaya, T. Baran, A. Mentes, M. Asaroglu, G. Sezen, K.Ö. Tozak, Extraction and characterization of α-chitin and chitosan from six different aquatic invertebrates, Food Biophys. (2014) 145–157.
[26] M. Kaya, S. Erdogan, A. Molb, T. Baran, Comparison of chitin structures isolated, from seven orthoptera species, Int. J. Biol. Macromol. 72 (2015) 797–805.
[27] M. Kaya, T. Baran, Description of a new surface morphology for chitin extracted from wings of cockroach (*Periplaneta americana*), Int. J. Biol. Macromol. 75 (2015) 7–12.
[28] M. Kabalaka, D. Aracagöka, M. Torunb, Extraction, characterization and comparison of chitins from large bodied four Coleoptera and Orthoptera species, Int. J. Biol. Macromol. 145 (2020) 402–409.

[29] C.-S. Shina, D.-Y. Kimb, W.-S. Shina, Characterization of chitosan extracted from Mealworm Beetle (Tenebrio molitor, Zophobas morio) and Rhinoceros Beetle (Allomyrina dichotoma) and their antibacterial activities, Int. J. Biol. Macromol. 125 (2019) 72–77.
[30] Y.-L. Huang, Y.-H. Tsai, Extraction of chitosan from squid pen waste by high hydrostatic pressure: effects on physicochemical properties and antioxidant activities of chitosan, Int. J. Biol. Macromol. 160 (2020) 677–687.
[31] J. Wu, Y. Niu, Y. Jiao, Q. Chen, Fungal chitosan from *Agaricus bisporus* (Lange) Sing. Chaidam increased the stability and antioxidant activity of liposomes modified with biosurfactants and loading betulinic acid, Int. J. Biol. Macromol. 123 (2019) 291–299.
[32] H. Looy, F.V. Dunkel Jr., How then shall we eat? Insect-eating attitudes and sustainable foodways, Wood, Agric. Hum. Values 31 (2014) 131–141.
[33] A. Van Huis, J. Van Itterbeeck, H. Klunder, E. Mertens, A. Halloran, G. Muir, P. Vantomme, Edible insects-future prospects for food and feed security, FAO Forestry Pap. 171 (2013) 1–187.
[34] G. Godeau, F. Orange, R.-P. Godeau, C.R. Szczepanski, F. Guittard, T. Darmanin, Structures and wettability in the genus Pachnoda Burmeister, Bioinsp. Biomim. Nanobiomat. 8 (2019) 181–189.
[35] G. Godeau, R.-P. Godeau, F. Orange, C.R. Szczepanski, F. Guittard, T. Darmanin, Variation of Goliathus orientalis (moser, 1909) elytra nanostructurations and their impact on wettability, Biomimetics 3 (2018) 6.
[36] P. Fournier, C.R. Szczepanski, R.-P. Godeau, G. Godeau, Chitosan extraction from *Goliathus orientalis* Moser, 1909: characterization and comparison with commercially available chitosan, Biomimetics 5 (2020) 15.
[37] O. Montreuil, C. Candet, A. Bonaccorso, C.R. Szczepanski, F. Orange, R.-P. Godeau, F. Guittard, T. Darmanin, G. Godeau, Micro- and nanoscopic observations of sexual dimorphisms in Mecynorhina polyphemus confluens (Kraatz, 1890) (Coleoptera, Cetoniidae, Goliathini) and consequences for surface wettability, Arthropod. Struct. Dev. 49 (2019) 10–18.
[38] R. Czechowska-Biskup, D. Jarosińska, B. Rokita, P. Ulański, J.M. Rosiak, Determination of degree of deacetylation of chitosan – comparision of methods, Prog. Chem. Appl. Chitin Deriv. 12 (2012) 5–20.
[39] R.A.A. Muzzarelli, Chitin, Pergamon Press, Oxford, 1977 105.
[40] N. H. Marei, E. Abd El-Samie, T. Salah, G. R. Saad, A. H. M. Elwahy, Isolation and characterization of chitosan from different local insects in Egypt. Int. J. Biol. Macromol. 82 (2016) 871–877.
[41] I. Younes, S. Hajji, V. Frachet, M. Rinaudo, K. Jellouli, M. Nasri, Chitin extraction from shrimp shell using enzymatic treatment. Antitumor, antioxidant and antimicrobial activities of chitosan, Int. J. Biol. Macromol. 69 (2014) 489–498.
[42] I. Younes, S. Hajji, V. Frachet, M. Rinaudo, K. Jellouli, M. Nasri, Preparation and characterization of α-chitin from cicada sloughs, Mater. Sci. Eng. C 30 (2010) 357–363.
[43] H. El Knidri, R. Belaabed, A. Addaou, A. Laajeb, A. Lahsini, Extraction, chemical modification and characterization of chitin and chitosan, Int. J. Biol. Macromol. 120 (2018) 1181–1189.
[44] J. Sebastiana, T. Rouissia, S.K. Brara, K.M. Hegdea, M. Vermac, Microwave-assisted extraction of chitosan from Rhizopus oryzae NRRL1526 biomass, Carbohydr. Polym. 219 (2019) 431–440.
[45] V. Allard, Les Coléoptères du Monde 6, Goliathini 2, Sciences Nat, Venette, France 1983, pp. 1–113.
[46] A.E. Seago, P. Brady, J.-P. Vigneron, T.D. Schultz, Gold bugs and beyond: a review of iridescence and structural colour mechanism in beetles (coleoptera), J. R. Soc. Interface 6 (2009) S165–S184.
[47] C.W. Mason, Structural colour in insects. I, J. Phys. Chem. 30 (1926) 383–395.
[48] C.W. Mason, Structural colour in insects. II, J. Phys. Chem. 31 (1927) 321–354.
[49] C.W. Mason, Structural colour in insects. III, J. Phys. Chem. 31 (1927) 1856–1872.
[50] J. Brugnerottoa, J. Lizardib, F.M. Goycooleab, W. ArguĚelles-Monalc, J. DesbrieÁresa, M. Rinaudo, An infrared investigation in relation with chitin and chitosan characterization, Polymer 42 (2001) 3569–3580.
[51] M. Lavertu, Z. Xia, A.N. Serreqi, M. Berrada, A. Rodrigues, D. Wang, M.D. Buschmann, A. Gupta, A validated 1H NMR method for the determination of the degree of deacetylation of chitosan, J. Pharm. Biomed. Anal. 32 (2003) 1149–1158.
[53] M. Nosonovsky, B. Bhushan, Biomimetic superhydrophobic surfaces: multiscale approach, Nano Lett. 7 (2007) 2633–2637.
[54] A. Sarkar, A.-M. Kietzig, Design of a robust superhydrophobic surface: thermodynamic and kinetic analysis, Soft Matter 11 (2015) 1998–2007.
[55] A. Giacomello, M. Chinappi, S. Meloni, C.M. Casciola, Metastable wetting on superhydrophobic surfaces: continuum and atomistic views of the Cassie-Baxter–Wenzel transition, Phys. Rev. Lett. 109 (2012) 226102/1–226102/4.
[56] L. Feng, Y. Zhang, J. Xi, Y. Zhu, N. Wang, F. Xia, L. Jiang, Petal effect: a superhydrophobic state with high adhesive force, Langmuir 24 (2008) 4114–4119.
[57] E. Bormashenko, T. Stein, R. Pogreb, D. Aurbach, "Petal effect" on surfaces based on lycopodium: high-stick surfaces demonstrating high apparent contact angles, J. Phys. Chem. C 113 (2009) 5568–5572.
[58] A. Marmur, Hydro- hygro- oleo- omni-phobic? Terminology of wettability classification, Soft Matter 8 (2012) 6867–6870.
[59] J.M. Yang, W.Y. Su, T.T. Leu, M.C. Yang, Evaluation of chitosan/PVA blended hydrogel membranes, J. Membr. Sci. 236 (2004) 39–51.
[60] F.I. Abou El Fadl, Radiation grafting of ionically crosslinked alginate/chitosan beads with acrylic acid for lead sorption, J. Radioanal. Nucl. Chem. 301 (2014) 529–535.
[61] X. Qi, S. Simsek, J.-B. Ohm, B. Chen, J. Rao, Viability of lactobacillus rhamnosus GG microencapsulated in alginate/chitosan hydrogel particles during storage and simulated gastrointestinal digestion: role of chitosan molecular weight, Softmater 16 (2019) 1877–1887.
[62] Z. Bagher, A. Ehterami, M. Nasrolahi, M. Azimi, M. Salehi, Hesperidin promotes peripheral nerve regeneration based on tissue engineering strategy using alginate/chitosan hydrogel: in vitro and in vivo study, Int. J. Polym. Mater. Polym. Biomater. (2020)https://doi.org/10.1080/00914037.2020.1713781.
[63] A. Suratman, A.D. Oktaviani, N.H. Aprilita, A.H. Wibowo, IOP Conf. Ser. Mater. Sci. Eng. 578 (2019), 012074. .